Heliyon 10 (2024) e35829

Contents lists available at ScienceDirect

Heliyon

journal homepage: www.cell.com/heliyon

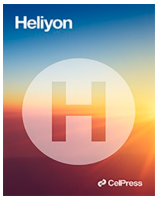

Research article

# Enhancing the photocatalytic efficiency of g-$C_3N_4$ for ciprofloxacin degradation using Tetrakis (acetonitrile) copper(I) hexafluorophosphate as a highly effective cocatalyst

Razieh Nejat

*Department of Chemistry, Kosar University of Bojnord, Bojnord, Islamic Republic of Iran*

ARTICLE INFO

*Keywords:*
Cu
G-$C_3N_4$
Photocatalyst
Antibiotic

ABSTRACT

Ciprofloxacin antibiotic (CP) is one of the antibiotics with broad-spectrum antimicrobial activity that has the highest rate of antibiotic resistance. This antibiotic undergoes incomplete metabolism within the human body and is excreted into the water, resulting in its hazardous biological and ecotoxicological effects. In this study, a novel photocatalyst, comprised of graphitic carbon nitride (g-CN) and Tetrakis(acetonitrile)copper(I)hexafluorophosphate ([$(CH_3CN)_4Cu]PF_6$), denoted as $CuPF_6$/g-CN, was employed for the degradation of ciprofloxacin under visible-light irradiation. The Cu complex, functioning as a co-catalyst, assumes a crucial role in facilitating the efficient separation of photogenerated charges and exhibiting high absorption in the visible-light region. More surprisingly, $CuPF_6$/g-CN does surpass by up to 6 times the behavior reached with bare g-CN. The experimental findings indicated that the optimal degradation of ciprofloxacin (CP) occurred after 50 min when using a concentration of 20 mg $L^{-1}$ CP and a concentration of 0.05 g/L $CuPF_6$/g-CN, under a pH of 8. This research offers valuable insights into the advancement of cost-effective co-catalysts that enhance the photocatalytic capabilities of established photocatalysts. It contributes to improving the overall performance and efficiency of these photocatalytic systems.

## 1. Introduction

Photocatalytic technology, being recognized as a highly favorable and promising process, holds great potential in addressing the escalating issue of water pollution. Through its safe and environmentally friendly approach, it offers an effective solution for the decomposition of organic pollutants, contributing to the mitigation of water pollution in a sustainable manner [1,2]. The core of the process of photocatalytic degradation is the design and fabrication of high-performance, eco-friendly, and economically viable photocatalytic materials. Materials with semiconductor properties are extensively employed as the predominant photocatalysts in various applications owing to their distinctive surface electronic, physical, chemical, optical, and redox properties [3]. g-CN as a metal-free and cost-effective organic semiconductor, stands out among these materials with its exceptional photocatalytic properties, due to great band structure, good thermal stability, non-toxicity, and tunable electronic structure [4,5].

Several studies have demonstrated that in comparison to bulk g-CN, the g-CN nanosheets (NS), have larger surface area and higher solubility in water and thus $C_3N_4$-NS have been applied in broad fields such as photocatalysis, electrochemical sensors, fuel cells, and fluorescence applications [6–11], Nevertheless, the large bandgap implying weak solar light absorption, the high photogenerated

*E-mail address:* organochem.nejat@kub.ac.ir.

https://doi.org/10.1016/j.heliyon.2024.e35829
Received 15 June 2024; Received in revised form 3 August 2024; Accepted 5 August 2024
Available online 15 August 2024

carrier recombination rate, and the inability to produce reactive species by the photogenerated holes ($h^+$) [12,13], hydroxyl radical have limited the use of g-CN in photocatalytic activity. One of the most significant strategies used to overcome these problems expressively and improve the effectiveness of g-CN photocatalysis is assembling the pristine g-CN with metal oxides [14], metallic elements [15], semiconductors [16,17], and magnetic nanoparticles [18].

In various methods explored, the use of co-catalysts is particularly important for simplifying the charge acceptance by species in solution and facilitating the redox reactions. Among several candidates, the heterojunction of g-CN with visible-light sensitizing Cu complex can be an excellent suggestion with a high absorption coefficient within the solar spectrum and low processing cost. Moreover, Cu metal is a cheap, nontoxicity, and abundant element [19,20], and the cu element has been investigated for photolysis application in various research [21–25].

On the other hand, the use of antibiotics as important clinical drugs has marked a new era of drugs for infectious illness therapy or other diseases in humans and animals [26,27]. The wide use of various antibiotics in order to treat infections and prevent diseases in animals has revolutionized in livestock, poultry, aquaculture, and cultivation industry [28–30]. However, arbitrarily and the overuse use of antibiotics leads to the production of untreated discharge and these antibiotic residues cause drug resistance which poses a significant threat to the ecological environment.

CP as a third generation and synthetic antibiotic belongs to the fluoroquinolone group of antibiotics which exhibits broad-spectrum antimicrobial activity but, unfortunately, CP is not able to be efficiently metabolized in the human body because of high structural stability, and thus, the residues are diffuse to the environment [31]. In addition, expired CP antibiotics as wastes are released into the natural environment [32] In general, the presence of CP in water and wastewater is a serious problem due to its toxicities and can accumulate in the organism.

In this research, we have synthesized ($[(CH_3CN)_4Cu]PF_6$) modified g-CN photocatalyst ($CuPF_6$/g-CN) for the destruction of CP in water in VIS light. Results show that the pure g-CN almost exhibits a partial reduction of CP concentration (about 10 %) during the photocatalytic process, and also, the photocatalytic performance of ($[(CH_3CN)_4Cu]PF_6$) salt, and g-CN modified with CuO was less of $CuPF_6$/g-CN. The results demonstrate the incorporation ($[(CH_3CN)_4Cu]PF_6$) molecules with g-CN resulted in improved light absorption spectrum of the carrier and photocatalytic activity due to its high surface area. Tetrakis(acetonitrile)copper(I) hexafluorophosphate is a useful source of unbound Cu(I).

## 2. Experimental section

All the materials, including thiourea, $HPF_6$, $CH_3CN$, ethanol, copper (I) oxide and acetonitrile were in analytic grade, prepared by Merck, Fluka, and Sigma-Aldrich chemical company, and used without further purification. X-ray diffractometry, XRD Philips PW1730 (using Cu Kα radiation (α = 0.154056 Å), was used for phase purity and crystalline structure analysis of samples. Fourier transform infrared spectra (NICOLET IR100 FT-IR with spectroscopic grade KBr) were obtained within the 400-4000 $cm^{-1}$ range. The Thermo Scientific Evolution 300/600 UV–Visible spectrophotometer (USA) was utilized to acquire the UV–vis diffuse reflectance spectra (DRS) of the samples. A Philips XL-300 was employed to perform the field emission scanning electron microscopy (FESEM) analysis. To determine the specific surface areas, the BET method was employed using the Micromeritics Instrument Corporation TriStar II. UV–visible absorption spectra were acquired at room temperature using a Shimadzu UV-2550-8030 spectrophotometer in the range 190–800 nm with a slit width of 5.0 nm. The light source employed had a wavelength of 360.0 nm. A 400 W lamp, specifically a high-pressure mercury-vapor lamp emitting light with a cutoff filter at 420 nm (SCF–S50-42 L; Sigma Koki, Japan., was utilized to provide the visible illumination.

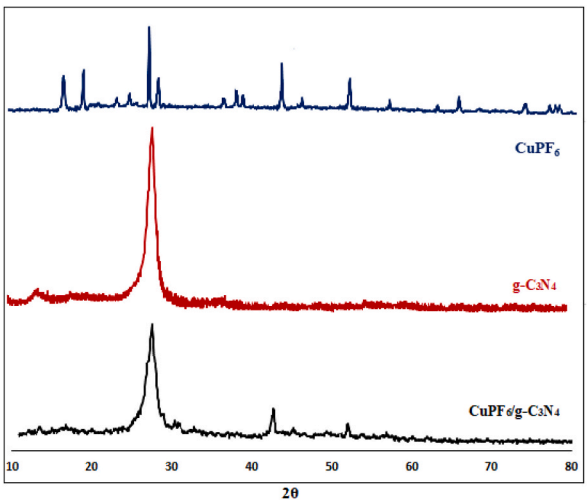


**Fig. 1.** XRD of g-CN, $CuPF_6$/g-CN and $CuPF_6$.

### 2.1. The synthesis of the photocatalyst

First, g-$C_3N_4$ was synthesized by annealing thiourea at 550 °C for 3 h with the heating rate of 5 °C $min^{-1}$ [33]. Tetrakis(acetonitrile) copper(I) hexafluorophosphate molecules were prepared following a previously published method [34]. To synthesize $CuPF_6$/g-CN, the g-CN (1.0 gr) in 60 ml of ethanol were added and sonicated (2 h) to make the thick slurry. Then, ($[(CH_3CN)_4Cu]PF_6$) (0.05 g) was added to the formed yellowish heterogeneous solution and for a duration of 24 h, the mixture underwent continuous stirring. In the final step, the cap was removed from the reaction vessel, and the solid phase was separated by filtration, it was then subjected to a drying process at 80 °C.

### 2.2. Characterization of the catalyst

Fig. 1 illustrates the XRD measurements of g-CN and $CuPF_6$/g-CN materials, shedding light on the presence, crystallinity degree, and purity of both g-CN and the catalyst. The X-ray diffraction (XRD) pattern of g-CN exhibited a prominent peak at $2\theta = 27.5°$, which corresponds to the (002) planes (JCPDS No. 87–1526). This peak is characteristic of the interplanar stacking structure commonly observed in graphitic materials [35,36]. Furthermore, a secondary diffraction peak at $2\theta = 13.1°$ was identified as corresponding to the (100) planes. The relatively good intensity of this peak provides further evidence for the presence of a graphite-like structure in the g-CN material [37–39]. Importantly, the characteristic peaks $[Cu(CH_3CN)_4]PF_6$ of g-CN remained weaker in the spectrum of the catalyst, indicating the successful loading of $[Cu(CH_3CN)_4]PF_6$ onto the g-CN material. The observed diminution in the intensity of the g-$C_3N_4$ diffraction peaks within the catalyst spectrum suggests the possibility of structural alterations to the g-$C_3N_4$ lattice arising from the modification process. Additionally, the emergence of new peaks at $2\theta = 43.3°$ and 50.4°, corresponds to the (111) and (200) planes of the elemental copper phase (JCPDS card 04–0836).

FT-IR spectroscopy was employed to analyze the molecular vibrations and functional groups of (2a) g-CN and (7b) $CuPF_6$/g-CN in the range of 400–4000 $cm^{-1}$ (Fig. 2). The chief peaks for pure g-CN appear between 1200 and 1700 $cm^{-1}$, corresponding to the stretching vibration of CN heterocycles. Another significant band is observed at 800 $cm^{-1}$, indicative of the breathing vibration of Tri-S-triazine units. The peaks in the range of 3150–3300 $cm^{-1}$ originate from the stretching vibration of N–H bonds [40]. In pure $[Cu(CH_3CN)_4]PF_6$ ($CuPF_6$), a prominent characteristic band is detected at 2427 $cm^{-1}$ which can be allocated to the vibration of the co-ordinated acetonitrile ligands. Additionally, the principal peaks observed within the range of 550–900 $cm^{-1}$ can be ascribed to the vibrational modes of the $PF_6$ counter ion (2c). The FT-IR spectrum of $CuPF_6$/g-CN retains all characteristic vibrational peaks of g-CN, including the bands attributed to CN bonds at 2327 and 2348 $cm^{-1}$. Additionally, distinct peaks corresponding to $PF_6$ vibrations are observed at 804 and 591 $cm^{-1}$ [41]. The presence of a small amount of $[Cu(CH_3CN)_4]PF_6$ on the g-CN material in the $CuPF_6$/g-CN spectrum leads to a reduced intensity of the specific g-CN bands. (Fig. 2b).

Fig. 3 illustrates the UV–Vis diffuse reflectance spectra (DRS) of the synthesized g-CN and $CuPF_6$/g-CN, providing insights into their respective optical properties. The addition of $[Cu(CH_3CN)_4]PF_6$ particles on the g-CN surface increased the absorbance of $CuPF_6$/g-CN. This higher absorbance indicates the generation of more electron-hole pairs under visible light, potentially enhancing the photo-activity of the material.

Fig. 4 showcases the SEM images of the g-CN support (Fig. 4a) and $CuPF_6$/g-CN catalyst, providing insights into their respective morphologies. In Fig. 4b, it is evident that the g-CN material is decorated with crystals, indicating successful loading of $[Cu(CH_3CN)_4]PF_6$ onto the g-CN support (Fig. 4b).

The successful incorporation of $[Cu(CH_3CN)_4]PF_6$ onto the surface of g-$C_3N_4$ is further evidenced by the TEM images presented in

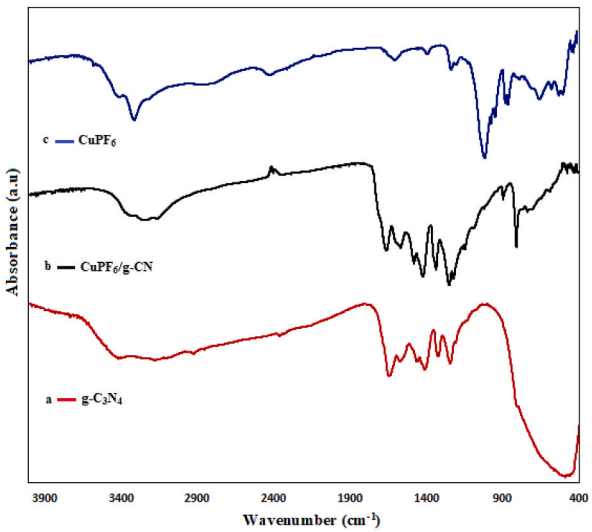


**Fig. 2.** FT-IR Analysis: (a) g-CN, (b) $CuPF_6$/g-CN and (c) $CuPF_6$ Spectra.

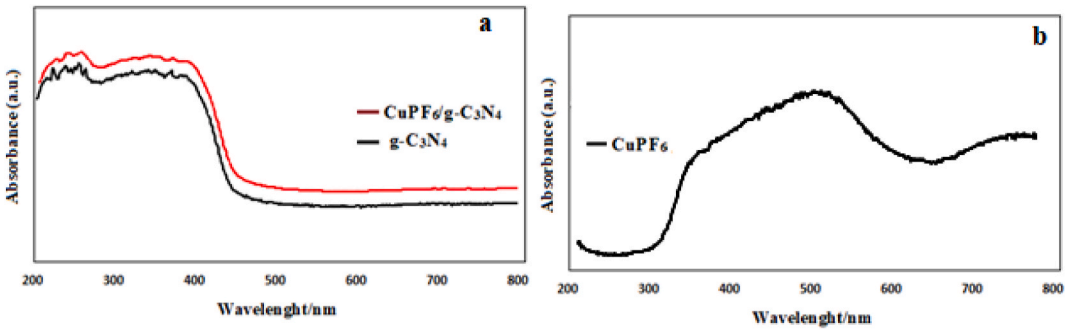


**Fig. 3.** UV–Vis DRS of a) g-CN, $CuPF_6$/g-CN, and b) $CuPF_6$.

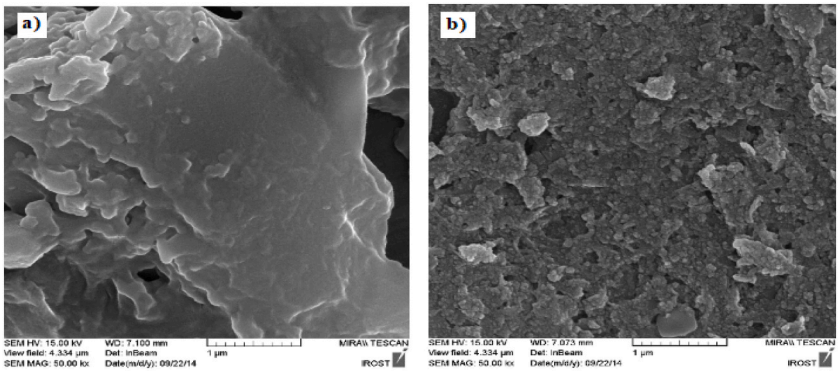


**Fig. 4.** SEM Analysis: (a) g-CN and (b) $CuPF_6$/g-CN Morphologies.

Fig. 5. This figure demonstrates that the $CuPF_6$/g-CN nanocomposite is composed of a significant quantity of $[Cu(CH_3CN)_4]PF_6$ particles, which occupy a substantial fraction of the available surface area on the g-$C_3N_4$ material. The g-$C_3N_4$ substrate serves as a matrix within which these $[Cu(CH_3CN)_4]PF_6$ particles are successfully integrated and uniformly distributed. This observation corroborates the effective integration and even dispersion of the $[Cu(CH_3CN)_4]PF_6$ species within the g-$C_3N_4$ matrix.

Energy-dispersive X-ray spectroscopy (EDS) was recorded and shown in Fig. 6. In the EDS spectrum of the catalyst, all the peaks related to Cu, P, C, N, and C were observed.

Nitrogen adsorption-desorption isotherm measurements were conducted to provide insights into the catalyst's pore structure and

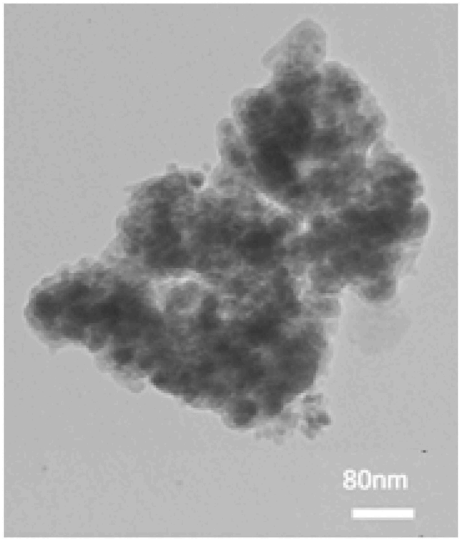


**Fig. 5.** TEM image of $CuPF_6$/g-CN.

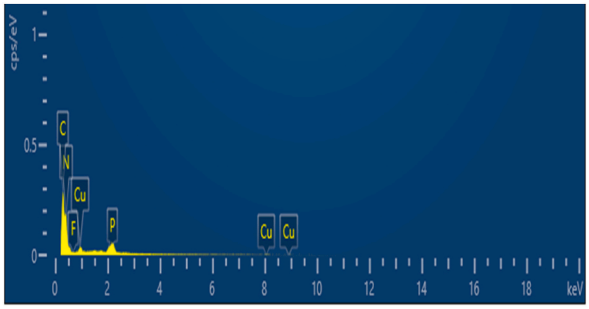


**Fig. 6.** EDS spectrum of the catalyst.

textural properties (Fig. 7). The nitrogen adsorption-desorption isotherms demonstrated a class IV mixture as per the IUPAC classification, characterized by a H3 hysteresis loop. The presence of hysteresis loops within the relative pressure range of 0.35–0.97 suggests that the samples possess a mesoporous structure in their porous network. As reported in previous studies, the pure g-CN material exhibited a low BET surface area of 10.2 $m^2/g$ [42,43] and after $[Cu(CH_3CN)_4]PF_6$ was loaded on g-CN, the BET surface area of g-CN experienced a significant increase to 17.64 $m^2/g$. The catalyst's specific surface area was determined using the BET method, yielding a value of (specific surface area value) $m^2/g$ (Fig. 7a). The pore size distribution was Pore size = 1.64 nm and a pore volume of 0.118 $cm^3/g$ (Fig. 7b).

Mott-Schottky plots were leveraged at a frequency of 500 Hz to scrutinize the band-edge potentials of the g-$C_3N_4$ and $CuPF_6$/CN photocatalysts (Fig. 8a). Fig. 8a displays the plots, and the positive slope observed in the curves denotes that both the g-$C_3N_4$ and $CuPF_6$/CN exhibit the characteristic n-type semiconductor behavior. As a result, the extrapolated conduction band (CB) positions of g-$C_3N_4$ and $CuPF_6$/CN samples stand at −0.95 V and −0.97 V, correspondingly (vs Ag/AgCl, pH = 7). Based on the band gaps of the g-$C_3N_4$ (2.84 eV) and $CuPF_6$/CN (2.59 eV), the valence band (VB) positions are calculated to be 1.62 V and 1.89 V, respectively. It was observed that the ECB changed to more negative for g-$C_3N_4$ after Cu modification, suggesting that $CuPF_6$/CN retained the strong redox ability of the photogenerated electrons. Fig. 8b displays electronic band structures for g-$C_3N_4$ and $CuPF_6$/g-CN.

The stability and recoverability of the catalyst were evaluated during the degradation of ciprofloxacin under visible-light irradiation. After each reaction, the catalyst was separated, washed with deionized water, dried, and then directly reused in the next run. It was observed that the recovered catalyst could be recycled in subsequent runs without a significant decrease in activity, even after the sixth run (Fig. 9).

### 2.3. Photocatalytic experiments

The evaluation of the photocatalytic activities of $CuPF_6$/g-CN involved using a catalyst mass of 0.05 g, 2 mmol of 33 % $H_2O_2$, and a reaction mixture containing 50 ml of an aqueous medium with a concentration of CP (20 mg $L^{-1}$). To maintain the adsorption-desorption equilibrium between CP and the catalyst surface, an adsorption reaction was initiated by subjecting the CP solution to magnetic stirring in the dark for a duration of 30 min. The solution was exposed to irradiation for a period of 50 min using a 400 W lamp (a high-pressure mercury vapor lamp emitting light at a wavelength of 546.8 nm). To avoid any potential thermal catalytic effects, the temperature of the photocatalytic reaction was carefully controlled and maintained between 25 and 30 °C. Cooling fans were employed to regulate and stabilize the temperature throughout the reaction. After 10 min, a sample of approximately 5 mL was extracted from the reaction mixture and subjected to centrifugation to separate the catalysts from CP. The resulting supernatant,

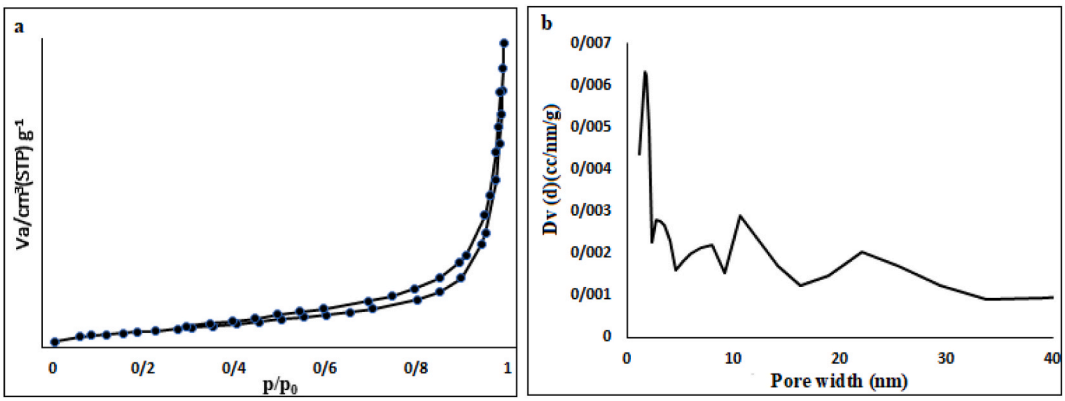


**Fig. 7.** $N_2$ sorption isotherms of photocatalyst (a), pore diameter distribution curve of photocatalyst (b).

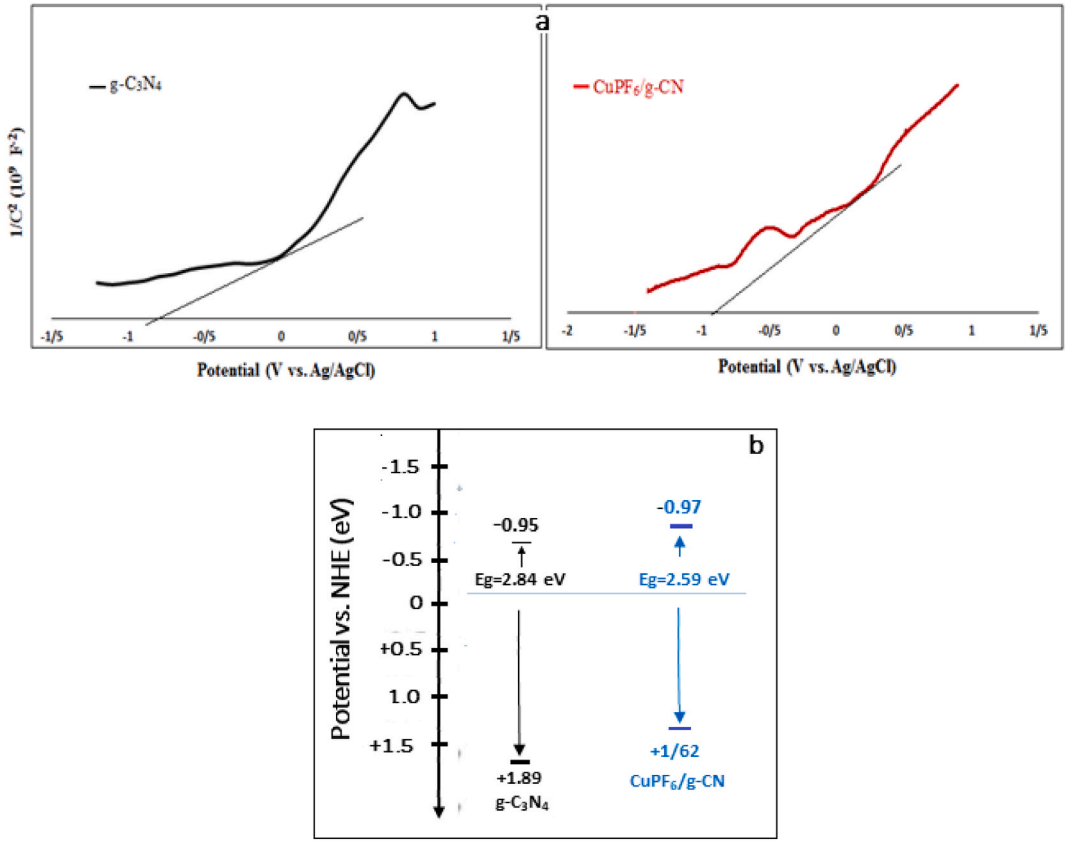


**Fig. 8.** (a) Mott-Schottky curves and (b) electronic band structures for g-$C_3N_4$ and $CuPF_6$/g-CN.

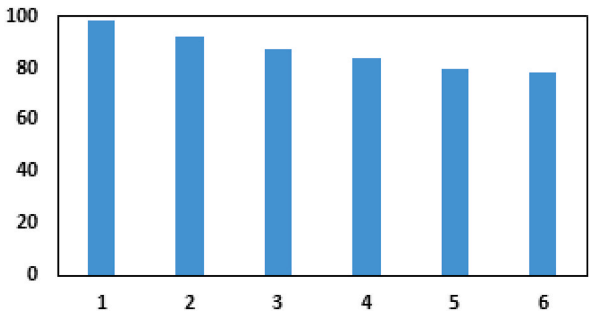


**Fig. 9.** Reusability of the $CuPF_6$/g-CN for degradation of ciprofloxacin under visible-light irradiation.

containing the CP, was measured by UV spectrophotometer.

Fig. 10 displays the UV–Visible absorption spectra of CP degradation using $CuPF_6$/g-CN under VIS light at pH 8. The spectra exhibit a maximum absorption band at 275 nm, indicating the absorption of light during the degradation process. Fig. 10 demonstrates the decrease in the absorption peak at 275 nm and the shoulder at 322 nm as the degradation progresses. After 50 min of irradiation, the degradation efficiency reached an impressive 98.5 %, indicating the successful photodegradation of CP using the photocatalyst.

Table 1 presents a comparison of the results from the current work with the results reported in similar articles investigating the degradation of antibiotics [44–49]

## 3. Results and discussion

### 3.1. Optimizing photocatalytic performance: reaction conditions for $CuPF_6$/g-CN composite

Fig. 11 showcases the combined effect of light irradiation and the catalyst on CP degradation, providing insights into their influence

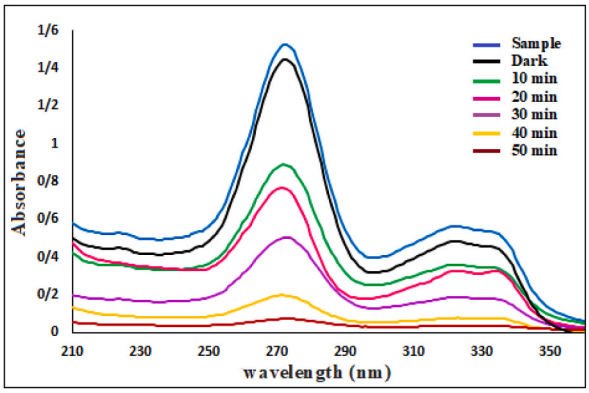


**Fig. 10.** UV–visible absorption spectra of CP elimination with $CuPF_6$/g-CN (CP) = 20 mg $L^{-1}$, [cat.] = 0.05 g, $H_2O_2$ (2 mmol), pH = 8).

**Table 1**
comparison of the results from the current work with the results reported in similar articles.

| Entry | Catalysts | Modification | Light source (lamp) | Band gap (eV) | Antibiotics (mg/L) | Performance over pristine g-$C_3N_4$ | Ref. |
|---|---|---|---|---|---|---|---|
| 1 | La-g-$C_3N_4$ | Metal doping | 18 UV (λ: 400–800 nm) | 2.63 | TC (10) | 5.6 | [44] |
| 2 | Cl-g-$C_3N_4$ | Non-metal doping | 300 Xenon (λ > 420 nm) | 2.70 | TC (10) | 2.4 | [45] |
| 3 | Er (III)-g-$C_3N_4$ | Metal doping | 35 W Xenon (−) | 2.4 | TC (25) | 1.7 | [46] |
| 4 | Ba-g-$C_3N_4$ | Metal doping | 150 W Xenon (λ > 400 nm) | 2.56 | TC (20) mg/L | 2.8 | [47] |
| 5 | Ag/g-$C_3N_4$ | Metal NPs decoration | 300 W Xenon (λ > 420 nm) | 2.72 | TC (20) | 3 | [48] |
| 6 | Cu/O-g-$C_3N_4$ | Co-doping | 300 W Xenon (λ > 420 nm) | 2.28 | LEVO (15) | 6.2 | [49] |

on the efficiency of the process. In the absence of the catalyst under visible (VIS) light irradiation, no degradation of CP is observed. However, a partial reduction in CP concentration (approximately 10 %) is observed when the catalytic reaction is conducted in the dark. This partial reduction is likely attributed to the partial adsorption of CP molecules onto the surface of the catalyst. The degradation efficiency is significantly enhanced up to 98.5 % when the CP solution containing the catalyst is exposed to visible (VIS) light irradiation.

Moreover, the effect of various VIS light-driven catalysts on CP degradation were examined (Fig. 12). The reference photocatalysts chosen for the study included CuO/g-CN, pristine g-CN, and $[Cu(CH_3CN)_4]PF_6$ salt, and their photoactivity was investigated by catalyzing the degradation of CP in water. Obviously, the photocatalytic activity of $CuPF_6$/g-CN was found to be significantly higher compared to pure g-CN and $[Cu(CH_3CN)_4]PF_6$ salt and also, $CuPF_6$/g-CN shows higher catalytic activity than CuO/g-CN for CP degradation under VIS light. This indicates that the introduction of the ($[(CH_3CN)_4Cu]PF_6$ salt enhances the photoactivity of the g-CN catalyst by absorbing well in the VIS light region, exhibiting superior adsorption towards CP molecules, and efficiently separating the photogenerated charges.

Fig. 13 demonstrates the influence of pH on the degradation of CP antibiotic in an aqueous solution. Based on the findings depicted in Fig. 13, the elimination of the CP at pH = 8 was complete after 50 min. The interaction strength between the catalyst and CP can

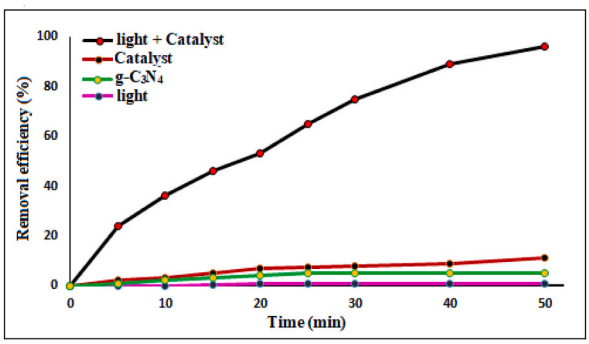


**Fig. 11.** Impacts of VIS light, g-CN, cat. and, (VIS light + cat.) on CP degradation.

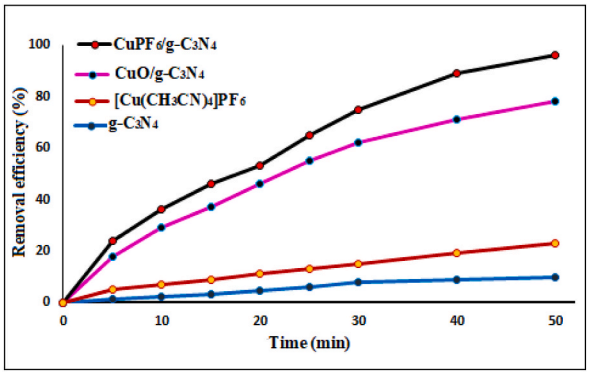


**Fig. 12.** Effects of various VIS light-driven catalysts on CP degradation.

influence the efficiency of Fenton reactions which is related to the pH conditions. Normally, CP molecules acquire positive and negative charges when introduced into acidic and basic solutions, because CP molecules accept and lose a hydrogen ion ($H^+$) respectively [50]. On the other hand, the acid-base properties of catalyst surfaces play a crucial role in governing the adsorption-desorption dynamics and the overall photocatalytic degradation performance [51]. pH levels ranging from 4 to 10 were investigated in the study. The degradation of CP is favored at slightly weak basic conditions because more CP molecules exhibit adsorption on the catalyst surface. The surface characteristics of catalysts play a crucial role as the reactions predominantly occur on their surfaces.

Fig. 14 demonstrates a positive correlation between the CP removal rate and the catalyst dosage within the range of 0.03 g/L to 0.15 g/L. The reaction exhibits the highest yield when utilizing 0.1 g of catalyst under VIS light irradiation, and reducing the amount of catalyst results in a decrease in yield, while further increasing the catalyst dosage leads to negligible improvement in the yield.

### 3.2. Possible oxidation mechanism

Herein, we report a postulated mechanism of combining our experiment results with related studies [52,53]. The results indicated that the coordination between $Cu^+$ and graphitic carbon nitride nanosheets resulted in enhanced generation of reactive oxygen species (ROS) upon exposure to light (Schemes 1 and 2). Probably, the integration of $Cu^+$ with g-CN would enhance the pro-oxidant effect. $Cu^+$–g-CN, serving as the redox-active species, exhibited the ability to catalyze the reduction of molecular oxygen to produce both superoxide anions and hydrogen peroxide. These reactive species, in turn, facilitated the generation of ROS, including the hydroxyl radical. It is observed that the reaction of the CP antibiotic with (OH) produced the $CO_2$, $H_2O$, and etc.

A series of control experiments were meticulously conducted to thoroughly investigate the pivotal reactive species involved in the photocatalytic degradation of CP in water by the $CuPF_6$/g-CN catalyst under sunlight. We strategically introduced various radical scavengers into the reaction system to selectively trap different reactive species. 1.0 mmol of KI, $AgNO_3$, ascorbic acid, and t-BuOH were carefully added to the reaction mixture to effectively trap holes ($h^+$), electrons ($e^-$), superoxide radicals ($^{\bullet}O^{2-}$), and hydroxyl radicals ($^{\bullet}OH$), respectively. It was observed that the incorporation of ascorbic acid and t-BuOH significantly impacted the degradation reaction rate of CP, while KI and $AgNO_3$ played a relatively diminished role in the photocatalytic activity compared to t-BuOH and ascorbic acid. These findings clearly and conclusively demonstrate that both $^{\bullet}O^{2-}$ and $^{\bullet}OH$ species are essential components in the photocatalytic oxidation process (Fig. 15).

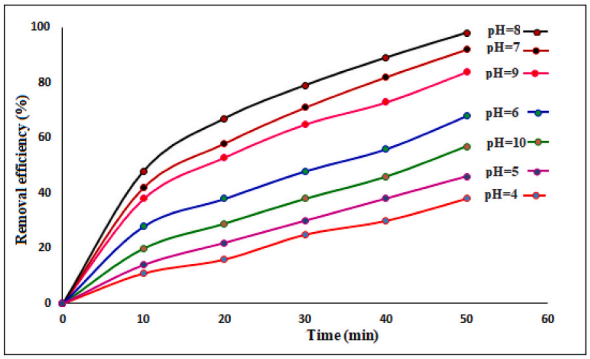


**Fig. 13.** Impact of Solution pH on CP Degradation in the Presence of $CuPF_6$/g-CN.

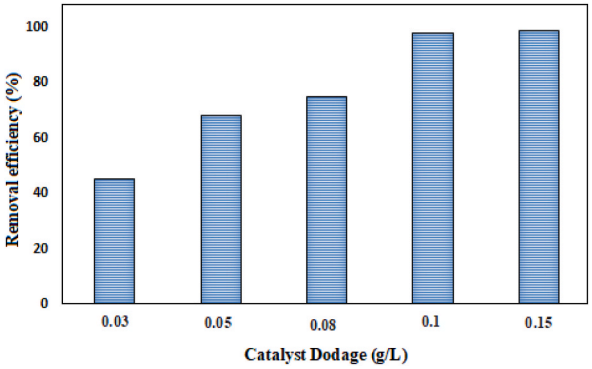


**Fig. 14.** Effect of the catalyst dosage for CP degradation by $CuPF_6$/g-CN.

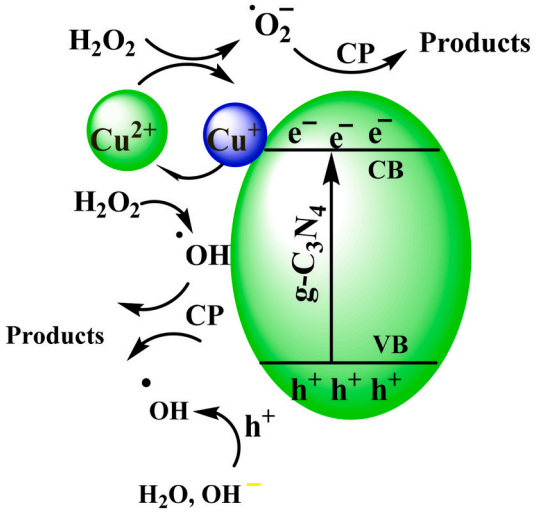


**Scheme 1.** The photocatalytic pathway of $CuPF_6$/g-CN under VIS light irradiation.

$$Cu^{+}/gC_3N_4 + H_2O_2 \longrightarrow {}^{\bullet}OH + OH^{-} + Cu^{2+}/gC_3N_4$$

$$Cu^{2+}/gC_3N_4 + H_2O_2 \longrightarrow Cu^{+}/gC_3N_4 + HO\text{-}O^{\bullet} + H^{+}$$

$$Cu^{2+} + gC_3N_4\,(e^{-}) \longrightarrow Cu^{+} + gC_3N_4\,(h^{+})$$

$$Cu^{2+}/gC_3N_4 + H_2O_2 \xrightarrow{h\nu} {}^{\bullet}O_2^{-} + Cu^{2+}/gC_3N_4 + H^{+}$$

$$CIP + {}^{\bullet}OH + {}^{\bullet}O_2^{-} + gC_3N_4\,(h^{+}) \longrightarrow \text{Products}$$

**Scheme 2.** Possible passway for the removal of CP under VIS light catalyzed by $CuPF_6$/g-CN.

## 4. Conclusions

In summary, the combination of g-CN with Tetrakis(acetonitrile)copper(I) hexafluorophosphate ($CuPF_6$/g-CN) resulted in the development of a highly effective photocatalyst. This photocatalyst exhibited exceptional performance in the removal of CP under VIS light irradiation. In this study, we evaluated the performance of g-CN, CuO/g-CN, $[(CH_3CN)_4Cu]PF_6$ salt, and $CuPF_6$/g-CN photocatalysts. Among these, $CuPF_6$/g-CN demonstrated superior effectiveness, exhibiting a CP elimination rate six times higher than that of g-CN. The presence of copper in the composite probably caused the reduction of the carrier recombination rate and the enhancement of photocatalytic degradation of CP. This project holds promise in providing an efficient and environmentally friendly technology for antibiotics treatment, utilizing $CuPF_6$/g-CN under VIS light.

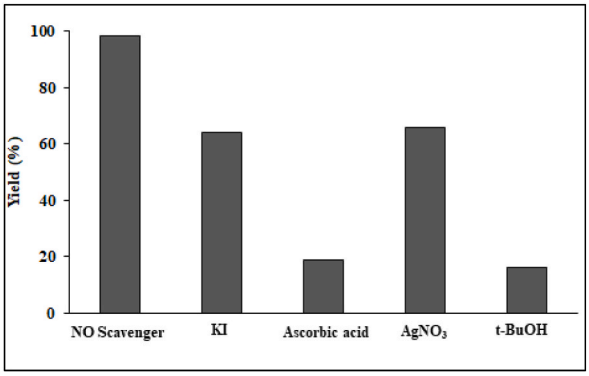


**Fig. 15.** The Impact of radical scavengers on the oxidation yields of CP Catalyzed by $CuPF_6/g\text{-}C_3N_4$.

## CRediT authorship contribution statement

**Razieh Nejat:** Writing – review & editing, Writing – original draft, Methodology, Investigation.

## Declaration of competing interest

The authors declare that they have no known competing financial interests or personal relationships that could have appeared to influence the work reported in this paper.

## Acknowledgement

Financial support of this work by Kosar University of Bojnord, Bojnord is gratefully acknowledged.

## References

[1] D. Ayodhya, G. Veerabhadram, Influence of $g\text{-}C_3N_4$ and $g\text{-}C_3N_4$ nanosheets supported CuS coupled system with effect of pH on the catalytic activity of 4-NP reduction using $NaBH_4$, Flat. Chem. 14 (2019) 100088, https://doi.org/10.1016/j.flatc.2019.100088.
[2] S.M. Flihh, S.H. Ammar, Fabrication and photocatalytic degradation activity of core/shell ZIF-67@ $CoWO_4$@ CoS heterostructure photocatalysts under visible light, Environ. Nano. Monit. Manag. 16 (2021) 100595, https://doi.org/10.1016/j.enmm.2021.100595.
[3] Y.S. Kareem, S.H. Ammar, R.A. Darwash, Microwave-induced catalytic oxidative desulfurization of gasoil fraction over phosphotungstic acid-based magnetic silica (Ni@ $SiO_2$\PWA) nanocatalyst, Catal. Commun. 136 (2020) 105926, https://doi.org/10.1016/j.catcom.2020.105926.
[4] A.I. Elaibi, S.H. Ammar, I.Sh Mohammed, Z.H. Jabbar, Construction of heteropolyacid-anchored magnetic $g\text{-}C_3N_4/Fe_3O_4$@polyindole hybrids for efficient photocatalytic destruction of methyl orange and bacteria, J. Photochem. Photobiol., A 444 (2023) 114923, https://doi.org/10.1016/j.jphotochem.2023.114923.
[5] R. Nejat, Z. Najminejad, F. Fazlali, S. Shahraki, Z. Khazaee, $g\text{-}C_3N_4/H_3PW_4Mo_8O_{40}$ S-scheme photocatalyst with enhanced photocatalytic oxidation of alcohols and sulfides, Inorg. Chem. Commun. 132 (2021) 108842, https://doi.org/10.1016/j.inoche.2021.108842.
[6] W.J. Ong, L.L. Tan, S.P. Chai, S.T. Yong, A.R. Mohamed, Surface charge modification via protonation of graphitic carbon nitride ($g\text{-}C_3N_4$) for electrostatic self-assembly construction of 2D/2D reduced graphene oxide (rGO)/$g\text{-}C_3N_4$ nanostructures toward enhanced photocatalytic reduction of carbon dioxide to methane, Nano Energy 13 (2015) 757–770, https://doi.org/10.1016/j.nanoen.2015.03.014.
[7] F. Salehnia, M. Hosseini, M.R. Ganjali, A fluorometric aptamer based assay for cytochrome C using fluorescent graphitic carbon nitride nanosheets, Microchim. Acta 184 (2017) 2157–2163, https://doi.org/10.1007/s00604-017-2130-6.
[8] Q. Zhao, H. Zhou, W. Wu, X. Wei, Sh Jiang, T. Zhou, D. Liu, Q. Lu, Sensitive electrochemical detection of tetrabromobisphenol A based on poly (diallyldimethylammonium chloride) modified graphitic carbon nitride-ionic liquid doped carbon paste electrode, Electrochim. Acta 254 (2017) 214–222, https://doi.org/10.1016/j.electacta.2017.09.114.
[9] J. Shi, M. Tai, J. Hou, Y. Qiao, C. Liu, T. Zhou, L. Wang, B. Hu, Intramolecular D-A structure and n-π* transition co-promoted photodegradation activity of carbon nitride: performance, mechanism and toxicity insight, Chem. Eng. J. 456 (2023) 141029, https://doi.org/10.1016/j.cej.2022.141029.
[10] Y. Wang, T. Zhou, H. Wang, L. Wang, J. Qi, K. Cui, C. Liu, B. Hu, Fabricating fragmented intramolecular D-A integrated carbon nitride photocatalyts with elevating activity: performance and mechanism analysis, Int J Hydrogen Energ 51 (2024) 61–71, https://doi.org/10.1016/j.ijhydene.2023.09.269.
[11] T. Zhou, G. Che, C. Liu, L. Ding, H. Teng, Recent advances on small molecule doped carbon nitride photocatalysts: application in environmental water remediation and clean energy production, Arab. J. Chem. 17 (2024) 105808, https://doi.org/10.1016/j.arabjc.2024.105808.
[12] J. Huang, X. Zhang, H. Song, C. Chen, F. Han, C. Wen, Protonated graphitic carbon nitride coated metal-organic frameworks with enhanced visible-light photocatalytic activity for contaminants degradation, Appl. Surf. Sci. 441 (2018) 85–98, https://doi.org/10.1016/j.apsusc.2018.02.027.
[13] Meng, T., Guangbo C., Tianyu, Zhou, Honghui, T., Chunbo, L., Bo, H., 2025. Tailoring C-defect O-doping and n-π* transition awakened porous ultra-thin carbon nitride for efficient peroxymonosulfate activation: Performances and mechanism insight. J. Environ. Sci. 152, 353-367. https://doi.org/10.1016/j.jes.2024.05.012.
[14] M.H. Fadhil, S.H. Ammar, M.F.A. Jabbar, Microwave-assisted catalytic oxidative desulfurization of gasoil fuel using synthesized CuO-ZnO nanocomposites, J. Fuel Chem. Technol. 47 (9) (2019) 1075–1082, https://doi.org/10.1016/S1872-5813(19)30044-1.
[15] L. Xu, S. Ling, H. Li, P. Yan, J. Xia, J. Qiu, K. Wang, H. Li, Sh Yuan, Photoelectrochemical monitoring of 4-chlorophenol by plasmonic Au/graphitic carbon nitride composites, Sens. Actuators B. chem. 240 (2017) 308–314, https://doi.org/10.1016/j.snb.2016.08.038.
[16] C. Li, H. Wu, D. Zhu, T. Zhou, M. Yan, G. Chen, J. Sun, G. Dai, F. Ge, H. Dong, High-efficient charge separation driven directionally by pyridine rings grafted on carbon nitride edge for boosting photocatalytic hydrogen evolution, Appl. Catal. B Environ. 297 (2021) 120433, https://doi.org/10.1016/j.apcatb.2021.120433.

[17] D. Chen, B. Li, Q. Pu, X. Chen, G. Wen, Z. Li, Preparation of Ag-$AgVO_3$/g-$C_3N_4$ composite photo-catalyst and degradation characteristics of antibiotics, J. Hazard Mater. 373 (2019) 303–312, https://doi.org/10.1016/j.jhazmat.2019.03.090.

[18] Sh Huang, Y. Xu, M. Xie, H. Xu, M. He, J. Xia, L. Huang, H. Li, Synthesis of magnetic $CoFe_2O_4$/g-$C_3N_4$ composite and its enhancement of photocatalytic ability under visible-light, Coll. Surf. A Physicochem. Eng. Asp. 478 (2015) 71–80, https://doi.org/10.1016/j.colsurfa.2015.03.035.

[19] W. Fa, L. Zan, C. Gong, J. Zhong, K. Deng, Solid-phase photocatalytic degradation of polystyrene with $TiO_2$ modified by iron (II) phthalocyanine, Appl. Catal. B Environ. 79 (3) (2008) 216–223, https://doi.org/10.1016/j.apcatb.2007.10.018.

[20] Z. Guo, B. Chen, M. Zhang, J. Mu, C. Shao, Y. Liu, Zinc phthalocyanine hierarchical nanostructure with hollow interior space: solvent–thermal synthesis and high visible photocatalytic property, J. Colloid Interface Sci. 348 (1) (2010) 37–42, https://doi.org/10.1016/j.jcis.2010.04.035.

[21] G. Pan, Z. Sun, Cu-doped g-$C_3N_4$ catalyst with stable $Cu^0$ and $Cu^+$ for enhanced amoxicillin degradation by heterogeneous electro-Fenton process at neutral pH, Chemosphere 283 (2021) 131257, https://doi.org/10.1016/j.chemosphere.2021.131257.

[22] L. Yang, X. Ren, Y. Zhang, Z. Chen, J. Wan, One-step synthesis of a heterogeneous catalyst: $Cu^+$-decorated triazine-based g-$C_3N_4$ nanosheet formation and catalytic mechanism, J. Envir. Chem. Engin. 9 (4) (2021) 105558, https://doi.org/10.1016/j.jece.2021.105558.

[23] X. Dou, Y. Chen, H. Shi, $CuBi_2O_4$/BiOBr composites promoted PMS activation for the degradation of tetracycline: S-scheme mechanism boosted $Cu^{2+}/Cu^+$ cycle, Chem. Engin. J. 431 (2022) 134054, https://doi.org/10.1016/j.cej.2021.134054.

[24] F. Abrishami, A. Soufi, M. Mahyari, Cu(I)@g-$C_3N_4$/PEI: a new heterogeneous catalyst for Glaser reaction in Deep Eutectic solvent, Cata. Let. (2023) 2989–3002, https://doi.org/10.1007/s10562-022-04188-9.

[25] G. Pan, Z. Sun, Cu-doped g-$C_3N_4$ catalyst with stable $Cu^0$ and $Cu^+$ for enhanced amoxicillin degradation by heterogeneous electro-Fenton process at neutral pH, Chem. Osph. 283 (2021) 131257, https://doi.org/10.1016/j.chemosphere.2021.131257.

[26] D. Chen, B. Li, Q. Pu, X. Chen, G. Wen, Z. Li, Preparation of Ag-$AgVO_3$/g-$C_3N_4$ composite photo-catalyst and degradation characteristics of antibiotics, J. Hazard Mater. 373 (2019) 303–312, https://doi.org/10.1016/j.jhazmat.2019.03.090.

[27] R. Davis, A. Markham, J.A. Balfour, Ciprofloxacin: an updated review of its pharmacology, therapeutic efficacy and tolerability, Drugs 51 (6) (1996) 1019–1074, https://doi.org/10.2165/00003495-199651060-00010.

[28] X. Chang, X. Yao, N. Ding, X. Yin, Q. Zheng, S. Lu, D. Shuai, Y. Sun, Photocatalytic degradation of trihalomethanes and haloacetonitriles on graphitic carbon nitride under visible light irradiation, Sci. Total Environ. 682 (2019) 200–207, https://doi.org/10.1016/j.scitotenv.2019.05.075.

[29] M. Kamagate, A.A. Assadi, T. Kone, S. Giraudet, L. Coulibaly, Kh Hanna, Use of laterite as a sustainable catalyst for removal of fluoroquinolone antibiotics from contaminated water, Chem. Osph. 195 (2018) 847–853, https://doi.org/10.1016/j.chemosphere.2017.12.165.

[30] A. Hassani, A. Khataee, S. Karaca, Photocatalytic degradation of ciprofloxacin by synthesized $TiO_2$ nanoparticles on montmorillonite: effect of operation parameters and artificial neural network modeling, J. Mol. Catal. Chem. 409 (2015) 149–161, https://doi.org/10.1016/j.molcata.2015.08.020.

[31] Y. Fei, Y. Li, Sh Han, J. Ma, Adsorptive removal of ciprofloxacin by sodium alginate/graphene oxide composite beads from aqueous solution, J. Colloid Interface Sci. 484 (2016) 196–204, https://doi.org/10.1016/j.jcis.2016.08.068.

[32] L. Li, J. Liu, J. Zeng, J. Li, Y. Liu, X. Sun, L. Xu, L. Li, Complete degradation and detoxification of ciprofloxacin by a micro-/nanostructured biogenic Mn oxide composite from a highly active $Mn^{2+}$-oxidizing pseudomonas strain, Nano. Mater. 11 (7) (2021) 1660, https://doi.org/10.3390/nano11071660.

[33] L. Ye, J. Liu, Z. Jiang, T. Peng, L. Zan, Facets coupling of BiOBr-g-$C_3N_4$ composite photocatalyst for enhanced visible-light-driven photocatalytic activity, Appl. Catal., B 142 (2013) 1–7, https://doi.org/10.1016/j.apcatb.2013.04.058.

[34] G.J. Kubas, B. Monzyk, A.L. Crumblis, Tetrakis (acetonitrile) copper (1+) hexafluorophosphate (1-), Inorg. Synth. 28 (1990) 68–70, https://doi.org/10.1002/9780470132593.ch15.

[35] J. Liu, T. Zhang, Z. Wang, G. Dawson, W. Chen, Simple pyrolysis of urea into graphitic carbon nitride with recyclable adsorption and photocatalytic activity, J. Mater. Chem. 21 (38) (2011) 14398–14401, https://doi.org/10.1039/C1JM12620B.

[36] F. Goettmann, A. Fischer, M. Antonietti, A. Thomas, Chemical synthesis of mesoporous carbon nitrides using hard templates and their use as a metal-free catalyst for Friedel–Crafts reaction of benzene, Angew. Chem., Int. Ed. 45 (27) (2006) 4467–4471, https://doi.org/10.1002/anie.200600412.

[37] S.C. Lee, H.O. Lintang, L. Yuliati, A urea precursor to synthesize carbon nitride with mesoporosity for enhanced activity in the photocatalytic removal of phenol, Chem. Asian J. 7 (9) (2012) 2139–2144, https://doi.org/10.1002/asia.201200383.

[38] K. Li, Z. Zeng, L. Yan, Sh Luo, X. Luo, M. Huo, Y. Guo, Fabrication of platinum-deposited carbon nitride nanotubes by a one-step solvothermal treatment strategy and their efficient visible-light photocatalytic activity, Appl. Catal., B 165 (2015) 428–437, https://doi.org/10.1016/j.apcatb.2014.10.039.

[39] S. Patnaik, S. Martha, G. Madras, K. Parida, The effect of sulfate pre-treatment to improve the deposition of Au-nanoparticles in a gold-modified sulfated g-$C_3N_4$ plasmonic photocatalyst towards visible light induced water reduction reaction, Phys. Chem. Chem. Phys. 18 (41) (2016) 28502–28514, https://doi.org/10.1039/C6CP04262G.

[40] G. Pan, Z. Sun, Cu-doped g-$C_3N_4$ catalyst with stable $Cu^0$ and $Cu^+$ for enhanced amoxicillin degradation by heterogeneous electro-Fenton process at neutral pH, Chem. Osph. 283 (2021) 131257, https://doi.org/10.1016/j.chemosphere.2021.131257.

[41] I.S. Kritchenkov, J.R. Shakirova, S.P. Tunik, Efficient one-pot green synthesis of tetrakis (acetonitrile) copper (I) complex in aqueous media, RSC Adv. 9 (27) (2019) 15531–15535, https://doi.org/10.1039/C8RA10564B.

[42] H. Sun, G. Zhou, Y. Wang, A. Suvorova, Sh Wang, A new metal-free carbon hybrid for enhanced photocatalysis, ACS Appl. Mater. Interfaces 6 (19) (2014) 16745–16754, https://doi.org/10.1021/am503820h.

[43] X. Wang, K. Maeda, A. Thomas, K. Takanabe, G. Xin, J.M. Carlsson, K. Domen, M. Antonietti, A metal-free polymeric photocatalyst for hydrogen production from water under visible light, Nat. Mater. 8 (1) (2009) 76–80, https://doi.org/10.1038/nmat2317.

[44] Ö. Tuna, E.B. Simsek, Synergic contribution of intercalation and electronic modification of g-$C_3N_4$ for an efficient visible light-driven catalyst for tetracycline degradation, J. Environ. Chem. Eng. 8 (5) (2020), https://doi.org/10.1016/j.jece.2020.104445.

[45] F. Guo, M. Li, M. Ren, X. Huang, K. Shu, W. Shi, C. Lu, Facile bottom-up preparation of Cl-doped porous g-$C_3N_4$ nanosheets for enhanced photocatalytic degradation of tetracycline under visible light, Sep. Purif. Technol. 228 (2019) 115770, https://doi.org/10.1016/j.seppur.2019.115770.

[46] G. Li, B. Wang, J. Zhang, R. Wang, H. Liu, Er-doped g-$C_3N_4$ for photodegradation of tetracycline and tylosin: high photocatalytic activity and low leaching toxicity, Chem. Eng. J. 391 (2020) 123500, https://doi.org/10.1016/j.cej.2019.123500.

[47] T.S. Bui, P. Bansal, B.K. Lee, T. Mahvelati-Shamsabadi, T. Soltani, Facile fabrication of novel Ba-doped g-$C_3N_4$ photocatalyst with remarkably enhanced photocatalytic activity towards tetracycline elimination under visible-light irradiation, Appl. Surf. Sci. 506 (2020) 1–12, https://doi.org/10.1016/j.apsusc.2019.144184.

[48] Z. Ren, F. Chen, K. Wen, J. Lu, Enhanced photocatalytic activity for tetracyclines degradation with Ag modified g-$C_3N_4$ composite under visible light, J. Photochem. Photobiol. Chem. 389 (2020) 112217, https://doi.org/10.1016/j.jphotochem.2019.112217.

[49] F. Li, P. Zhu, S. Wang, X. Xu, Z. Zhou, C. Wu, One-pot construction of Cu and O co-doped porous g-$C_3N_4$ with enhanced photocatalytic performance towards the degradation of levofloxacin, RSC Adv. 9 (2019) 20633–20642, https://doi.org/10.1039/c9ra02411e.

[50] M.E. Roca Jalil, M. Baschini, K. Sapag, Influence of pH and antibiotic solubility on the removal of ciprofloxacin from aqueous media using montmorillonite, Appl. Clay Sci. 114 (2015) 69–76, https://doi.org/10.1016/j.clay.2015.05.010.

[51] D. Chen, A.K. Ray, Photodegradation kinetics of 4-nitrophenol in $TiO_2$ suspension, Water Res. 32 (11) (1998) 3223–3234, https://doi.org/10.1016/S0043-1354(98)00118-3.

[52] Q. Ding, F.L.Y. Lam, X. Hu, Complete degradation of ciprofloxacin over g-$C_3N_4$-iron oxide composite via heterogeneous dark Fenton reaction, J. Environ. Manage. 244 (2019) 23–32, https://doi.org/10.1016/j.jenvman.2019.05.035.

[53] T.Y. Lin, C.Z. Zhu, P. Zhang, Y. Wang, H.H. Wu, J.J. Feng, J. Zhang, Regiodivergent intermolecular [3+ 2] cycloadditions of vinyl aziridines and allenes: stereospecific synthesis of chiral pyrrolidines, Angew. Chem. 128 (36) (2016) 11002–11006, https://doi.org/10.1002/ange.201605530.